APPENDIX B

Potential rockfall-generated tsunami at Whittier, Alaska

by
D.J. Nicolsky[1], G.J. Wolken[2], R.A. Combellick[2], and R.A. Hansen[1]

Introduction

During summer 2011, scientists from the Alaska Division of Geological & Geophysical Surveys (DGGS) conducted geologic-hazards fieldwork around Passage Canal and discovered a number of mass-movement features, including several rockfalls along the steep slopes of Passage Canal. A large subaerial rockfall entering into Passage Canal has the potential to generate a local tsunami that could impact the community of Whittier and damage critical infrastructure.

The destructive effects of mass-movement-generated tsunamis have been previously identified in south-central and southeastern Alaska. The best known and largest subaerial mass-movement-generated tsunami of historic time occurred in Lituya Bay, Alaska, on June 9, 1958, when a magnitude 7.9 earthquake occurred on the nearby Fairweather fault and produced an estimated 30 million m^3 (1,050 million ft^3) rockfall that rapidly entered the water and initiated a tsunami with the highest wave ever recorded (524 m/1,700 ft) (Miller, 1960).

In light of recent field observations indicating the potential for a large subaerial rockfall into Passage Canal, and to provide guidance to local emergency management agencies in tsunami hazard assessment, we append this brief report that considers an additional hypothetical rockfall-generated tsunami scenario in Passage Canal.

Aerial and field observations

A large bedrock fracture with a downhill-facing scarp was identified above the north shore of Passage Canal (figs. B-1 and B-2). The fracture is located above an active rockfall, characterized by intermittent toppling of rock

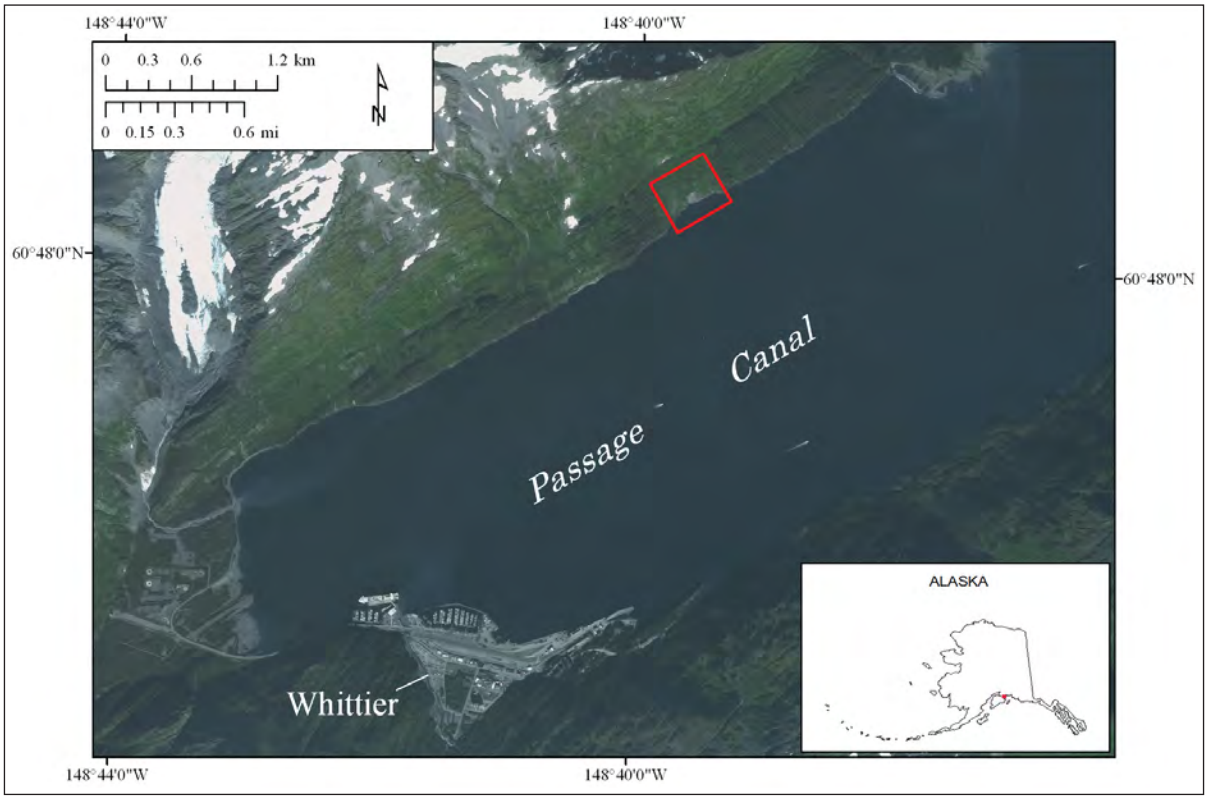

Figure B-1: *2010 SPOT satellite image of western Passage Canal and Whittier, Alaska. The red box indicates the location of the main rockfall and bedrock fracture.*

[1]Alaska Earthquake Information Center, Geophysical Institute, University of Alaska, P.O. Box 757320, Fairbanks, Alaska 99775-7320
[2]Alaska Division of Geological & Geophysical Surveys, 3354 College Rd., Fairbanks, Alaska 99709-3707

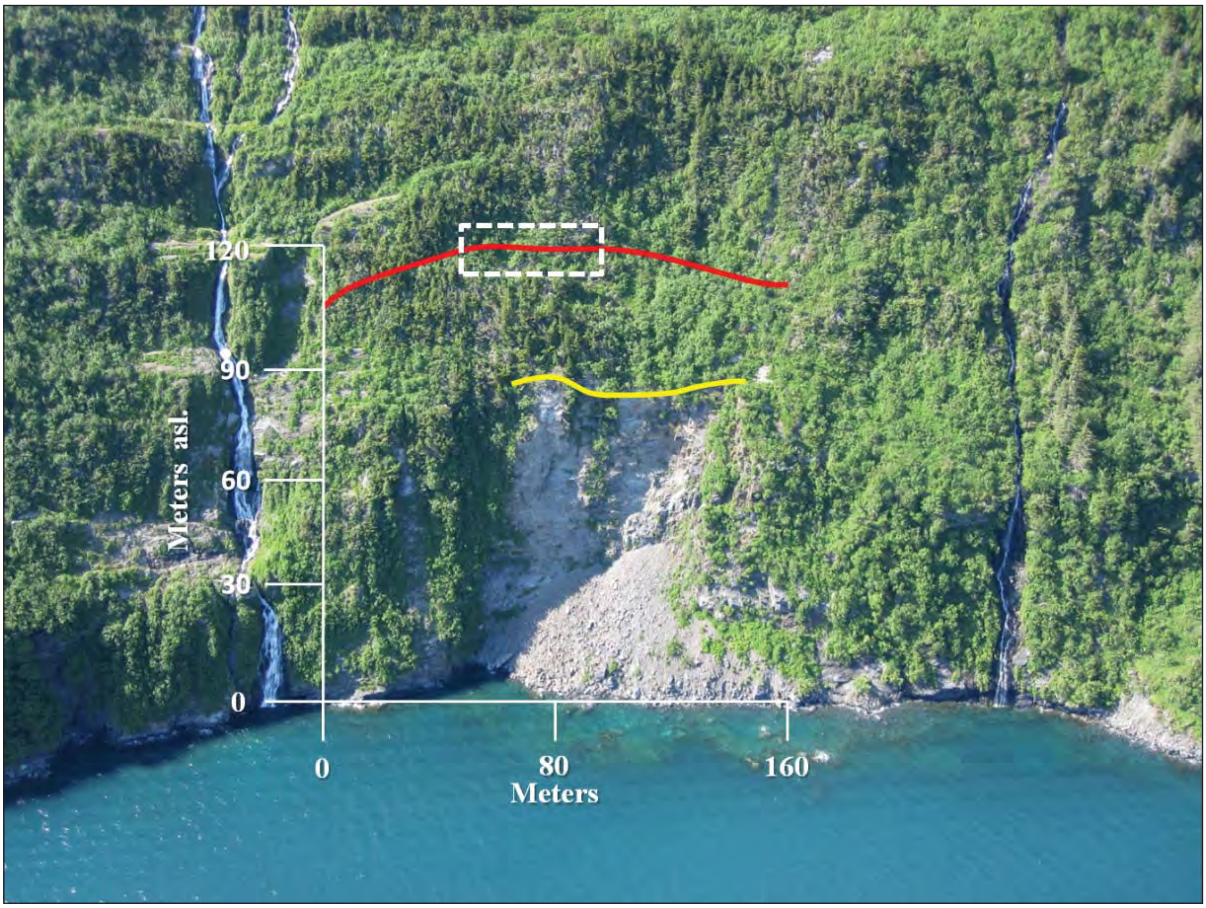

Figure B-2: *Photograph of the main rockfall and fracture above the north shore of Passage Canal. The yellow line shows the active scarp of the rockfall, the red line shows the position of the bedrock fracture, and the dashed white box indicates the location of the photographs in figure B-4.*

debris ranging from small fragments to boulders up to 3 m (10 ft) in diameter. The fracture exhibits relatively less weathering and oxidation compared to surrounding rocks and remains free of vegetation (fig. B-3), suggesting a relatively recent formation. Although no exact age is known, analysis of historic aerial photographs and satellite imagery indicates that the scarp occurred between 1950 and 1978.

The bedrock fracture is approximately 55 m (180 ft) above the active rockfall scarp, or approximately 120 m (400 ft) above sea level. It is mostly obscured by dense vegetation and is only visible from the air, mostly in areas of snow-avalanche scars. Views of the fracture from the air and ground are shown in figure B-3. Combined ground and aerial observations indicate that the fracture width ranges from 1.75 to 2.25 m (5.7–7.4 ft) and its length is about 160 m (520 ft). While the full length of the fracture remains unknown, the estimated surface area between the active rockfall scarp and observed fracture is near 6,200 m^2 (67,000 ft^2). The fracture has an arcuate convex-up form, suggesting that its origin could be related to the mechanisms influencing the active rockfall below. No other cracks are visible between the fracture and active rockfall scarp, indicating that the bedrock block below the fracture may have detached rigidly in response to the removal of lateral support from the mountain slope (glacier debuttressing), possibly in combination with external stimuli, such as seismic activity, rapid snowmelt, and intense rainfall.

We emphasize that the field observations of the depth of the fracture, and hence the total thickness of the material that can fail, are inconclusive. The fracture is located in a broad snow-avalanche zone where rock and vegetation are regularly transported down slope, resulting in avalanche debris lodged in the fracture. The debris forms an intermittent false “floor” at a 2 m (7 ft) depth, obscuring the true depth. On the basis of these surface measurements, it is estimated that a volume of the potential rockfall is considerably less than that of the 1958 Lituya Bay rockfall.

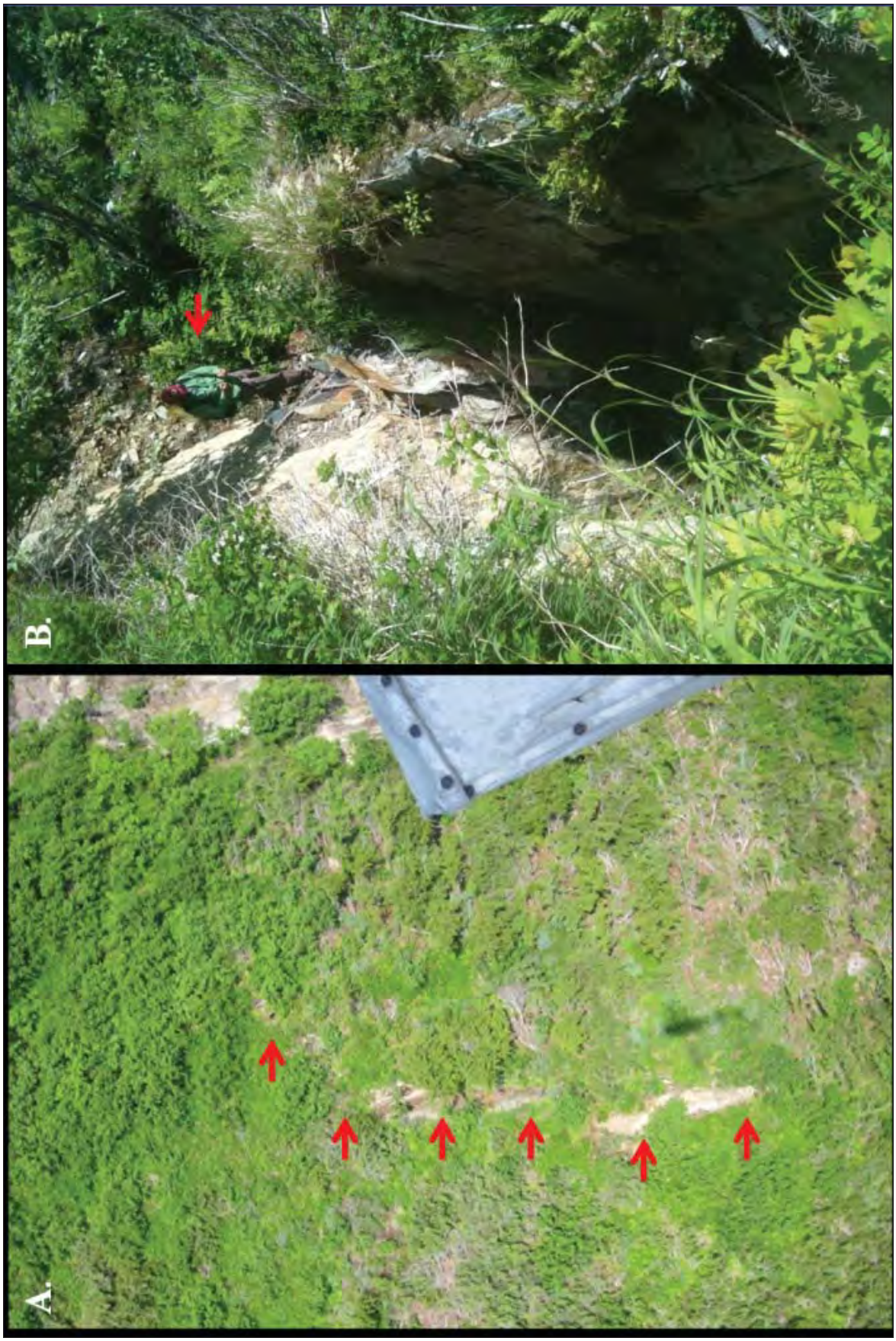

Figure B-3: *Photograph of the bedrock fracture from the air (A) and the ground (B). Red arrows in A show the location of the fracture; red arrow in B identifies a person for scale.*

Methodology and data

Our ability to accurately model effects of a potential rapid subaerial mass failure into Passage Canal and the subsequent impact of the rockfall-generated tsunami on Whittier depends on our knowledge of the type and geometry of the mass movement and the local bedrock geology. Dense vegetation covers the slope on which the fracture is located; as a result, the total length and geometry of the fracture is currently unknown. Moreover, in the absence of drilling and seismic profiling, the volume of the detached ground material is undetermined. Thus, the rockfall-generated tsunami scenario presented below represents our best estimate based on the currently available information.

Hypothetical rockfall tsunami source

An aerial view of the rockfall is shown in figure B-4. The red line in this figure marks the hypothesized extent of the potential rockfall. Based on field observations, we assume that the upper limit of the potential rockfall is constrained by the bedrock fracture (figs. B-2 and B-3). The lateral extent of the potential rockfall was assumed based on extension of the arcuate form of the fracture. Note that the upper limit coincides with the surveyed extent of the fracture, the location of which is shown by a series of white triangles representing GPS measurements. The lower boundary of the rockfall is assumed here to be located well below the water surface. The green line dissects the area roughly in half and is used to illustrate hypothetical failure surfaces along the transect XY. Because the subsurface geologic data are missing, we calculated two hypothetical failure scenarios in order to give a range of variability in the modeled run-up.

In figure B-5, Cases A (red) and B (green) represent failure curves along the transect XY. The upper boundary of the rockfall is placed at the fracture, or ~ 120 m (400 ft) above the water, while the lower boundary is assumed to be 60 m (200 ft) below the water surface. We estimate that in Case A the total volume of the hypothetical rockfall is approximately 1.2 million m^3 (42 million ft^3), while in Case B the estimated volume is 1.8 million m^3 (63 million ft^3). We emphasize that these volumes are rough estimates, and further research is necessary to refine these values.

Numerical modeling

Modeling of waves generated by a rapid failure of the fjord slope presents a major difficulty in the tsunami-hazard assessment. An impact of the rockfall on the water surface results in a turbulent splash and consequent mixing of the granular flow with water. As the rockfall material submerges, a non-linear interaction of the sliding rockfall material with water further shapes the generated tsunami.

Typically, there are several regions with distinct tsunami features considered around the rockfall. In the splash zone, a turbulent and chaotic water behavior (Fritz, 2002) can be modeled up to a certain extent by the 3-D Navier–Stokes equations coupled with an appropriate model of the slide (Heinrich, 1992; Heinrich and others, 1998). The choice of slide model depends on the type of the ground material and its rheology. Beyond the splash zone, in the so-called near-field zone, chaotic waves evolve into a well defined wave that propagates away from the slide. Finally, the far-field zone is characterized by a steady partitioning of the kinematic and potential energy and by a well defined wave form.

Identifying these zones is a complicated task and involves both theoretical and experimental studies (Mei, 1983; Fritz, 2002; Walder and others, 2006). On other hand, if the splash zone is much smaller than the distance to a location where the run-up needs to be assessed, then it is common to assume that the splash zone is a ‘black box’ (Walder and others, 2006). The water wave is thought to be emerging from the ‘black box’ with well defined characteristics, that is, the wave exiting the splash zone is approximated by a soliton (Watts and Waythomas, 2003; Waythomas and others, 2006) or a parabola (Wieczorek and others, 2007). The initial wave height is parameterized by its slide volume, density, thickness, and velocity when the slide plunges into the water.

Instead of determining an initial wave profile (for example, the shape of the soliton), we assume that, to a certain extent, the rockfall can be approximated by a viscous slide that generates a tsunami. The dynamics of the sub-aerial part of the rockfall are modeled incorrectly, but the errors introduced are probably no greater than those introduced if the initial wave profile were specified as mentioned above. The simulated wave height 15 seconds after the failure, estimated for Case B, is shown in figure B-6. In a cross-section, the computed wave resembles a soliton and most of its energy is directed perpendicular to the shore. According to numerical modeling experiments, the rockfall is almost completely submerged 15 seconds after the failure and its further interaction with water is simulated by a viscous slide model coupled with the long-wave approximation for water waves. The model description[3] is provided in Section “Numerical model of landslide-generated tsunami waves.” We emphasize that along with the numerical modeling assumptions in the splash zone, geometry and configuration of the rockfall introduces most of the uncertainties in the presented modeling.

[3]The rockfall density is assumed to be 2,700 kg/m^3 (170 lb/ft^3).

The potential tsunami can reach Whittier in approximately one and one-half minute after the failure. The wave height in Passage Canal at Point 17, which is just outside of the Whittier harbor, is estimated to be about 2 m (7 ft). Most of the inundation is localized in the eastern part of the city near the small harbor. However, according to numerical experiments, the wave breakers are over-topped and a limited inundation within the harbor parking area is also expected. The modeled extents of the inundation in Rockfalls A and B are shown in figure B-7, by red and green lines, respectively. The sea level dynamics and water velocities at the inundated locations are plotted in figure B-8. The maximum wave height is approximately 3 m (10 ft) at Point 5. The waves can reach 1.5 m (5 ft) in the Whittier harbor, but subside after several erratic oscillations.

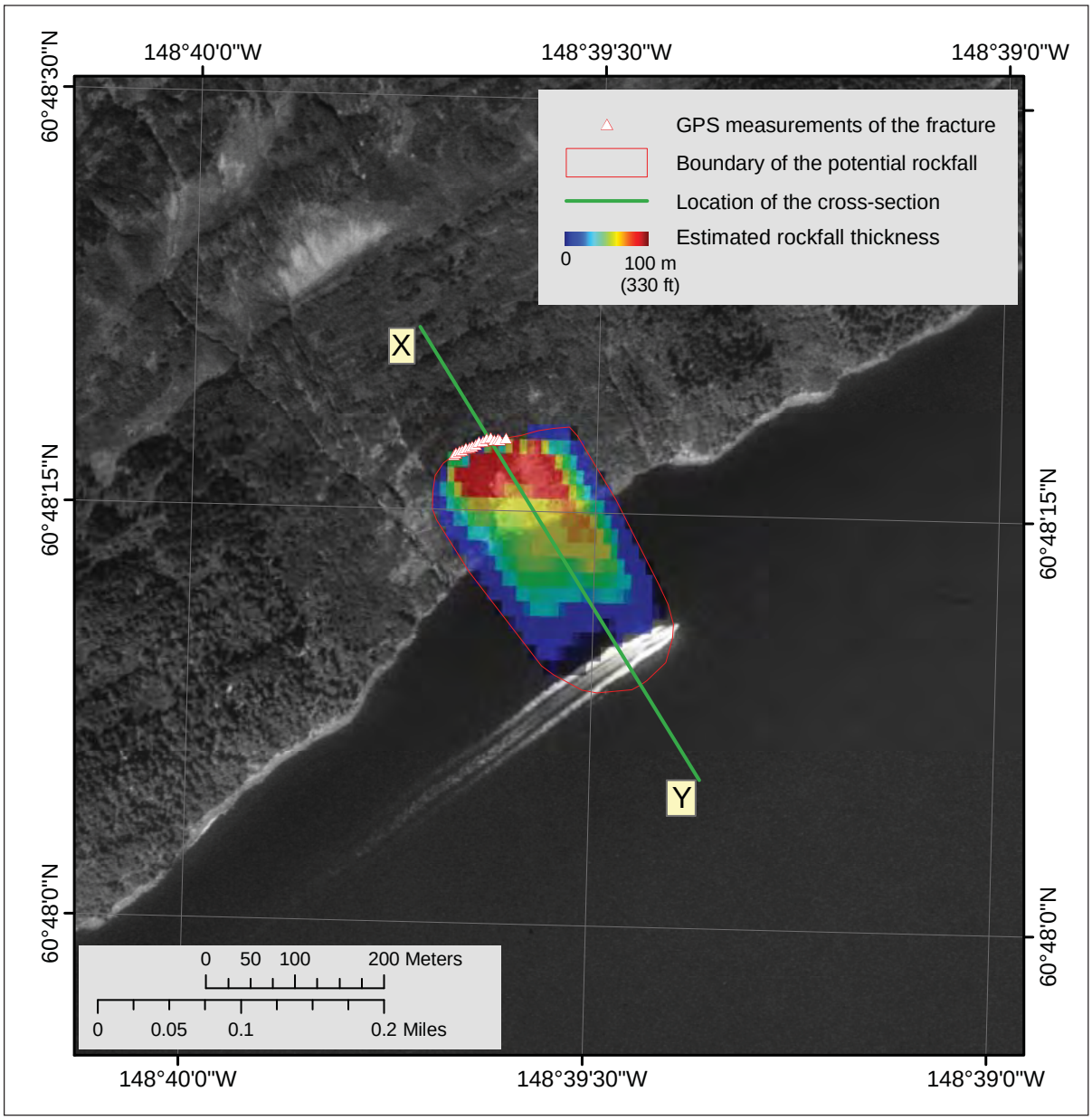

Figure B-4: *Aerial view of the study area with the red line showing an extent of the potential rockfall. GPS locations of a visible part of the fracture are marked by white triangles. The green line shows a transect, along which two cases of the hypothetical failure surfaces are proposed (see figure B-5). The thickness of the rockfall, estimated for Case B, is shown on top of the image. The maximum thickness is approximately 70 m (230 ft) near the fracture.*

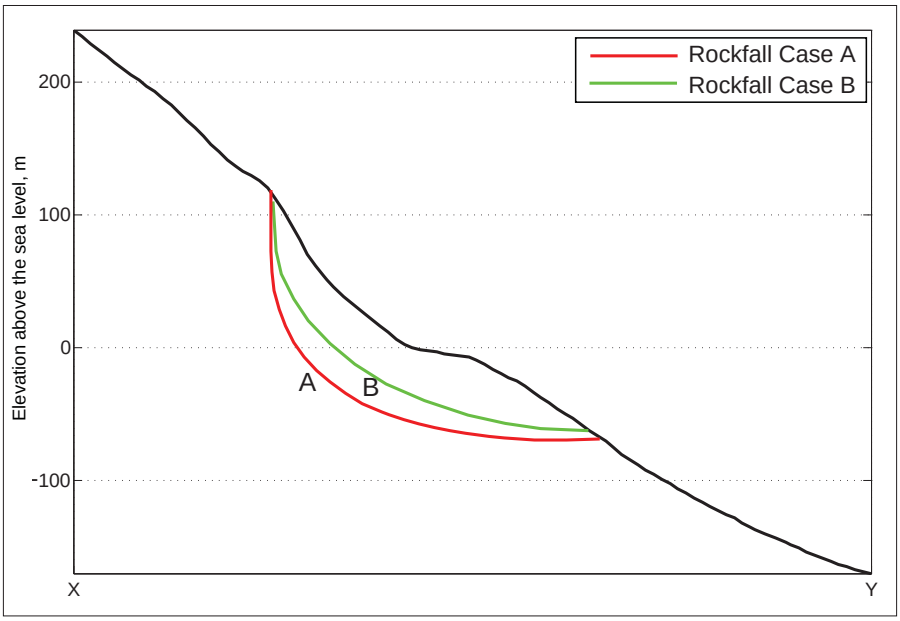

Figure B-5: *Failure surfaces along the transect XY plotted by a green line in figure B-4.*

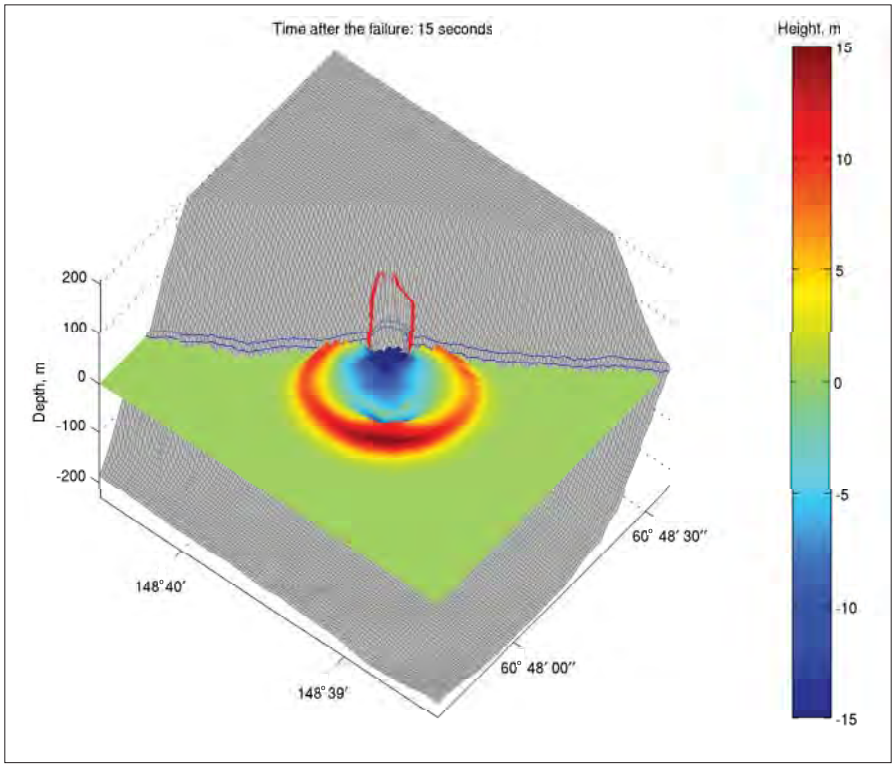

Figure B-6: *Numerically modeled wave leaving the splash zone 15 seconds after the rockfall failure. The extent of the rockfall is marked by a red line. The blue lines correspond to 0 and 10 m (33 ft) elevations above the sea level. The DEM corresponds to the present-day MHHW datum. For the sake of visualization, the elevations are cut at the 200 m (660 ft) level.*

Sources of errors and uncertainties

The hydrodynamic model used to calculate tsunami propagation and run-up is a nonlinear, flux-formulated, shallow water model (Nicolsky and others, 2011). It passed the validation and verification tests required for models used in production of tsunami inundation maps (Synolakis and others, 2007). In a series of papers, several numerical methods, based on Boussinesq-type approximation, were developed (Madsen and others 1991; Kirby and others 1998). However, the advantage of the latter models over classical shallow-water equations in matching field observations is an active area of research (Lynett and others, 2003; Tappin and others 2008).

Volume and configuration of the potential slope failure, dynamics of the rockfall, as well as the rheological properties of the sliding material are the largest uncertainties in the presented tsunami modeling study. Thus, additional in situ measurements and future modeling efforts are required to address these uncertainties.

References Cited

Fritz, H.M., 2002, Initial phase of landslide generated impulse waves: Zürich, Switzerland, Swiss Federal Institute of Technology (ETH), Ph.D. dissertation.

Heinrich, Philippe, 1992, Nonlinear water waves generated by submarine and aerial landslides: Journal of Waterway, Port, Coastal, and Ocean Engineering, v. 118, p. 249–266.

Heinrich, Philippe, Mangeney, Anne, Guibourg, Sandrine, Rocher, Roger, Boudon, Georges, and Cheminee, Jean-Louis, 1998, Simulation of water waves generated by a potential debris avalanche in Montserrat, Lesser Antilles: Geophysical Research Letters, v. 25, no. 19, p. 3,697–3,700.

Kirby, J.T., Wei, G., Chen, Q., Kennedy, A.B., and Dalrymple, R.A., 1998, FUNWAVE 1.0, Fully nonlinear Boussinesq wave model; Documentation and user's manual: Report CACR-98-06, Center for Applied Coastal Research, Department of Civil and Environmental Engineering, University of Delaware.

Lynett, P.J., Borrero, J.C., Liu, P.L.F., and Synolakis, C.E., 2003, Field survey and numerical simulations—A review of the 1998 Papua New Guinea tsunami, *in* Bardet, Jean-Pierre, Synolakis, C.E., Davies, H.L., Imamura, Fumihiko, and Okal, E.A., eds., Landslide tsunamis; Recent findings and research directions: Basel, Switzerland, Birkhaeuser, Pure and Applied Geophysics, v. 160, no. 10–11, p. 2,119–2,146.

Madsen, P.A., Murray, Russel, and Sorensen, O.R., 1991. A new form of the boussinesq equations with improved linear dispersion characteristics: Coastal Engineering, v. 15, no. 4, p. 371–388.

Mei, C.C., 1983, The Applied Dynamics of Ocean Surface Waves: John Wiley & Sons, 760 p.

Miller, D.J., 1960, Giant Waves in Lituya Bay, Alaska: U.S. Geological Survey Professional Paper 354-C, p. 51–86, 1 sheet, scale 1:50,000.

Nicolsky, D.J., Suleimani, E.N., and Hansen, R.A., 2011, Validation and verification of a numerical model for tsunami propagation and runup: Pure and Applied Geophysics, v. 168, p. 1,199–1,222, http://dx.doi.org/10.1007/s00024-010-0231-9.

Synolakis, C.E., Bernard, E.N., Titov, V.V., Kânoğlu, U., and González, F.I., 2007, Standards, criteria, and procedures for NOAA evaluation of tsunami numerical models: Seattle, Washington, NOAA/Pacific Marine Environmental Laboratory, Technical Memorandum OAR PMEL-135, 55 p.

Tappin, D.R., Watts, Philip, and Grilli, S.T., 2008, The Papua New Guinea tsunami of 17 July 1998—Anatomy of a catastrophic event: Natural Hazards and Earth System Sciences, v. 8, no. 2, p. 243–266.

Walder, J.S., Watts, P., and Waythomas, C.F., 2006, Case study: Mapping tsunami hazards associated with debris flow into a reservoir: Journal of Hydraulic Engineering, v. 132, no. 1, p 1–11.

Watts, P., and Waythomas, C.F., 2003, Theoretical analysis of tsunami generation by pyroclastic flows: Journal of Geophysical Research, B, Solid Earth and Planets, v. 108, p. 21.

Waythomas, C.F., Watts, P., and Walder, J.S., 2006, Numerical simulation of tsunami generation by cold volcanic mass flows at Augustine Volcano, Alaska. Natural Hazards and Earth System Science, v. 6, no. 5, p. 671–685.

Wieczorek, G.F., Geist, E.L., Motyka, R.J., and Jakob, M., 2007, Hazard assessment of the Tidal Inlet landslide and potential subsequent tsunami, Glacier Bay National Park, Alaska: Landslides, v. 4, p. 205–215.

Figure B-7: *Modeled potential inundation by the rockfall-generated waves, for two different cases. The volume in Rockfall A is 1.8 million m³ (63 million ft³) and in Rockfall B is 1.2 million m³ (42 million ft³). The DEM corresponds to the present-day MHHW datum. Because of the steep topography, inundation areas for several tsunami scenarios have a common boundary, and the plotted extents of the inundation areas may overlay each other.*

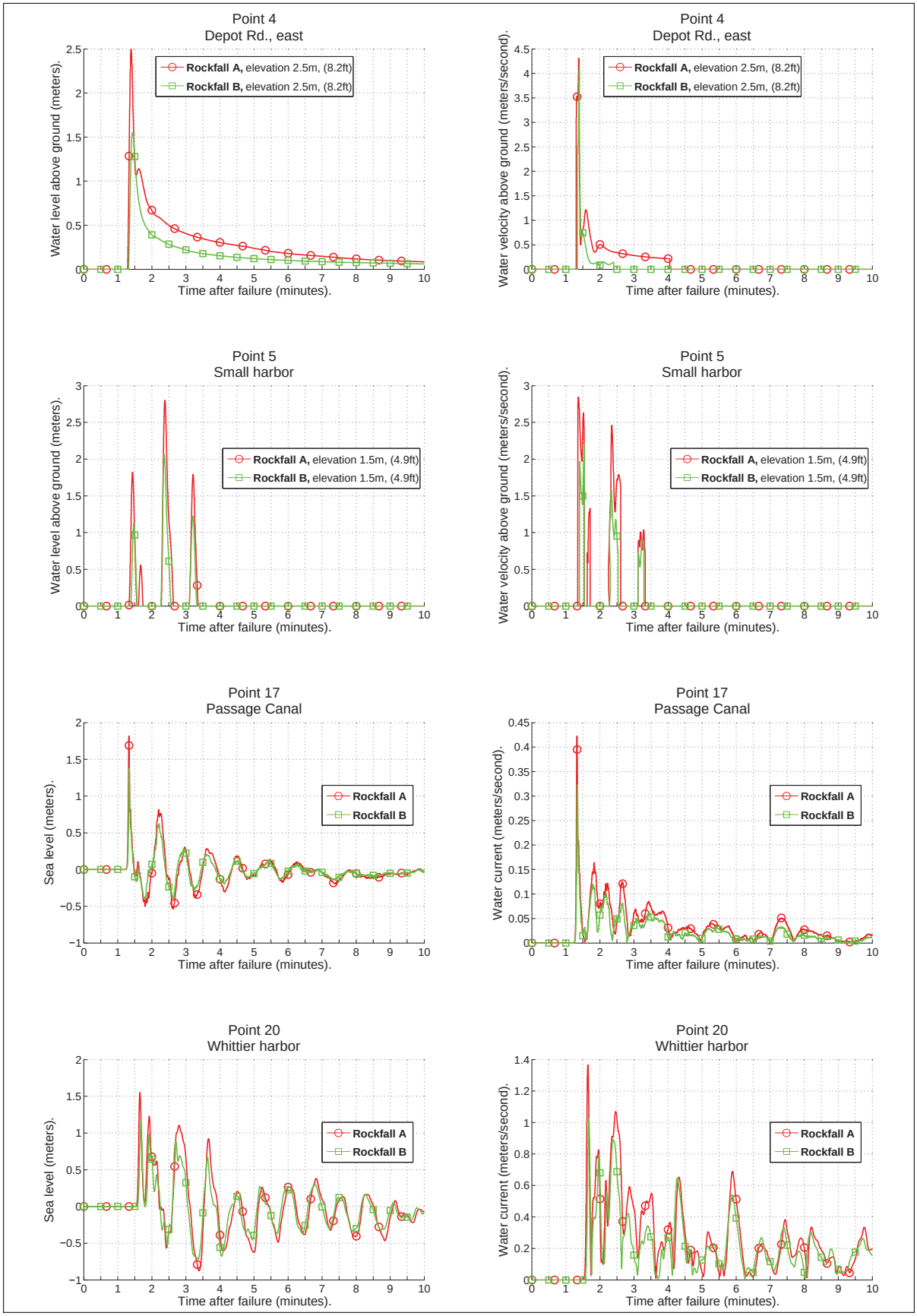

Figure B-8: *Time series of the water level and velocity at the selected points in Rockfalls A and B. Location of the points are shown in figure A-1.*